Characterization of Sorption Isotherms, Kinetic Models, and Multivariate Approach for Optimization of Hg(II) Adsorption onto *Fraxinus* Tree Leaves

Javad Zolgharnein* and Ali Shahmoradi

Department of Chemistry, Faculty of Science, Arak University, Arak 38156-8-8349, Iran

Statistical experimental design was utilized to optimize removal of aqueous Hg(II) by *Fraxinus* tree leaves through a batch biosorption process. Sorbent−sorbate behavior was evaluated by fitting equilibrium data by nonlinear and transformed linear forms of the Langmuir, Freundlich, and Redlich−Peterson isotherms. The comparative study showed that nonlinear regression is a better way to model equilibrium data. A 2^3 full factorial design was used to identify significant factors and interactions. The pH, Hg(II) initial concentration, and sorbent mass were examined as major factors. The contact time was fixed at 30 min. All of the factors were significant at the 95 % confidence level. The amount of Hg(II) was determined by cold vapor atomic absorption spectrophotometry. A regression model was derived by using a response surface methodology through performing central composite design (CCD). Model adequacy was checked by such diagnostic tests as analysis of variance (ANOVA), lack of fit test, residuals distribution, and over-fitting test. On the other hand a residuals distribution was evaluated for normality according to the Ryan−Joiner test. As a result, the optimized condition for Hg(II) biosorption was calculated to be pH = 4.4, s = 0.25 g, and m = 50 mg·L^{-1}, which corresponds to 92.25 % removal efficiency. The biosorption process was kinetically fast and followed a pseudosecond order kinetic model. Fourier transform infrared (FT-IR) and X-ray diffraction (XRD) spectra were used to find more about the biosorption mechanism.

Introduction

Mercury enters the environment from a large number of sources related to human use of heavy metals. Mercury has known harmful effects for human health and biota. Air, water, and soil can be polluted by mercury and its various compounds.[1,2] Therefore, the safe and efficient removal of mercury has critical importance. Although mercury discharge into aquatic systems has been largely prohibited, there are still a lack of efficient and low-cost methods for such wastewater treatment containing mercury. Traditional methods for metal ion removal such as precipitation, ion exchange, and activated carbon adsorption have techno-economical limitations.[3,4] When the pollutant concentration is very small, this problem is more important.[5] Hence biosorption processes are successful alternatives for heavy metal removal and the sorption ability of many living[6] and nonliving biosorbents including dried plant leaves,[5,7,8] roots,[9,10] papaya wood,[11] algae,[12] coffee grounds,[13] microorganisms,[14] and so forth, have been examined. There are only a few reports for removal of Hg(II) by biosorbents, especially using tree leaves which are cheap and easily available in a great supply.[4,5,7,8,13−17] There is also a lack of systematic multivariate optimization of Hg(II) biosorption conditions in the literature. It is recognized that a conventional optimization method has serious restrictions, and multivariate optimization through experimental design strategy approaches has many advantages.[8,18−24] In this approach, a response surface methodology leads to an empirical model which is related to the removal of a metal ion with effective variables and their interactions.[8,18,22] There are few reports that use experimental design methodology as an optimization tool for the removal of heavy metal ions by agricultural residues.[8,16,25−30] This study verified the potential of *Fraxinus* tree leaves as a new biosorbent for the removal of Hg(II) from aqueous waste. The experimental design methodology was also applied to do multivariate optimization of Hg(II) adsorption onto *Fraxinus* tree leaves. Furthermore, central composite design (CCD) was used as a response surface approach to find optimum conditions for maximum removal of Hg(II) from aqueous solution. The sorbent−sorbate equilibrium behavior through fitting experimental data to the major isotherm models was evaluated. The best fitting conditions of the isotherm models using both linear and nonlinear approaches were also examined. Additionally the kinetics of the biosorption process was studied.

Experimental Section

Biosorbent Material. *Fraxinus* tree leaves were gathered from twigs into clean plastic bags washed with doubly distilled water and were dried on a clean table. The dried leaves were ground well and sieved to (40 to 50) mesh, then stored in a plastic bag.

Metal Solution. A 1000 mg·L^{-1} stock solution of Hg(II) was prepared by dissolving appropriate quantities of $HgCl_2$ salt in 5 % (v/v) HNO_3 to avoid hydrolysis of $NaBH_4$, which was used as a reducing agent. All of the chemicals were analytical grade and obtained from Merck (Darmstadt, Germany). Doubly distilled water was used throughout. In a typical run, 50 mL of Hg(II) solution was used, and a known amount of dried biomass was added to each sample solution. The pH of solution was adjusted with HNO_3 or NaOH before the addition of biosorbent. Fresh dilutions were made for each study. Primary experiments show that the biosorption

* Corresponding author. E-mail: j-zolgharnein@araku.ac.ir.

10.1021/je1006218
Published on Web 09/29/2010

Table 1. Factor Names and Their Levels Used in the Factorial Design

variable	name	factor levels		
		−1	0	1
m	Hg(II) initial concentration ($mg \cdot L^{-1}$)	50	175	300
s	sorbent mass (g)	0.05	0.15	0.25
pH	solution pH	2	3.5	5

process of Hg(II) by *Fraxinus* tree leaves is very fast at the initial stage and reaches equilibrium at about (15 to 25) min, and further time does not have much effect on the removal efficiency.[6] So, the contact time was chosen to be 30 min. The samples were filtered to remove settled and suspended solid particles.

Procedure. The concentration of Hg(II) remaining in solution after biosorption was determined through a cold vapor atomic absorption spectrophotometric method using a Perkin-Elmer (2380 system) and MHS 20 unit. The instrumental conditions were adjusted as recommended by the manufacturer (wavelength 253.6 nm with a spectral bandwidth of 0.7 nm).

Consequently eqs 1 and 2 have been utilized for determining the removal percent (R) and amount of adsorbed Hg(II) (q) by the biomass from aqueous solution.

$$R = 100(m_i - m_f)/m_i \quad (1)$$

$$q = (m_i - m_f)V/s \quad (2)$$

where m_i ($mg \cdot L^{-1}$) is the initial concentration, m_f ($mg \cdot L^{-1}$) is the final concentration of the Hg(II) in the solution, q is the amount of Hg(II) taken up by the biosorbent ($mg \cdot g^{-1}$), V is the volume of solution (L), and s is the weight of biomass (g).

FT-IR and XRD Analysis. Fourier transform infrared (FT-IR) spectra of biomass before and after mercury biosorption in the range (400 to 4000) cm^{-1} were taken by using a Unicam-Galaxy series FT-IR 5000 to identify functional groups of *Fraxinus* tree leaves and possible Hg(II) binding sites. In addition, an X-ray diffraction (XRD) pattern of the pristine and Hg(II) loaded biosorbent were recorded using a Philips X-ray diffractometer (model PW 3040/60 X'pert pro).

Experimental Design Strategy. Screening Design. In many cases there may be a lot of factors that seems to be important, but in reality only a few of them control the response in a significant way. The primary goal of screening designs is to identify the few factors or key variables that influence the response. It is necessary to reduce the number of experiments and save time and cost. For this reason, a full 2^3 factorial design was performed. The factors considered were pH of solution, sorbent mass (s), and initial mercury concentration (m). Table 1 shows the factors and their levels. The design also has three replicates at the center point, allowing us to check curvature in the response surface model.[19,20]

Response Surface Design. The response surface approach is desirable to find a mathematical model capable of predicting the response. The optimized model was obtained by using the CCD. To do this, one should measure the response at some points of the working domain. The selection of these experimental points needs prior knowledge and should be done carefully to map the experimental domain correctly. There are statistically developed designs which determine in what points of space the experiments should be performed. Box-Behenken, CCD, and Doehlert design lie in this category.[19−23] In the current study, CCD was used as the optimization approach. Through running CCD, a regression model was fitted to the response (removal percent). Such tests as lack of fit, analysis of variances (ANOVA), analysis of residuals distribution, over-fitting test, and coefficient of determination (R^2) were used to check the adequacy of the model.[18−24] All of the statistical and mathematical calculations were done by using Minitab version 15 and Maple version 9.5, respectively. One can calculate the optimized condition by a visual or mathematical technique and compare theoretical and practical responses, when a suitable model has been found.

Isotherm Study. Three isotherms, the Langmuir, Freundlich, and Redlich−Peterson models, were fitted to the experimental data to find out more details of the process, including maximum theoretical adsorption capacity, mechanism of process, physiosorption or chemisorption, monolayer or multilayer adsorption, and so forth.[31,32] To make a comparison, the isotherm parameters were calculated by linear and nonlinear regression methods.[33−36]

Linear Regression Analysis. Linear regression using a least-squares method has been frequently used in the literature to determine adjustable parameters of isotherms. To do this, the isotherms are transformed into a linear form and then subjected to linear regression.[33,34] Despite simplicity, simple linear regression will result in different parameter estimations depending on which linearized form is used.[36] This is because each transformation changes the original error distribution function differently and this makes selection of the "really best fitted isotherm" difficult. It is suggested that the highest coefficient of determination (R^2) does not necessarily imply the best fit, but rather, the model having the error distribution most closely similar to the "true error distribution". The preferred transformation therefore may be different from data set to data set.[34] In fact, if the coefficient of determination of the transformed model is used as a measure to judge the fitness of the untransformed original model, then incorrect conclusions may be obtained. The Langmuir isotherm can be linearized as four different types as listed in Table 2. The parameters of the isotherms are denoted as: K_L is the Langmuir biosorption constant relating the free energy of biosorption. The q_{eq} and q_m values are used for monolayer equilibrium and maximum biosorption capacity, respectively. The Langmuir isotherm assumes the uptake of metal ions on a homogeneous surface by monolayer adsorption without any interaction between adsorbed ions. K_F is the Freundlich constant, where K_F is a constant relating the biosorption capacity and $1/n$ is an empirical parameter relating the biosorption intensity. It varies with the heterogeneity of the material and has a higher value for more heterogeneous surfaces. A, B, and g are the Redlich−Peterson isotherm constants.

Nonlinear Regression Analysis. All of the nonlinear model parameters were evaluated by nonlinear regression analysis using the SPSS 15 software. To quantitatively compare the applicability of each model a normalized standard deviation (Δq) is calculated as follows.[37]

$$\Delta q = \sqrt{\frac{\sum [(q_{e,exp} - q_{e,cal})/q_{e,exp}]^2}{n - 1}} \quad (3)$$

where n is the number of data points and q_e is the sorbent capacity at the equilibrium experimental conditions ($q_{e,exp}$) and calculated ($q_{e,cal}$), respectively. Since Δq represents agreement

Table 2. Isotherms and Their Linear Forms

isotherm		linear form	plot
Freundlich	$q_{eq} = K_F C_{eq}^{1/n}$	$\log(q_{eq}) = \log(K_F) + 1/n \log(C_{eq})$	$\log(q_{eq})$ vs $\log(C_{eq})$
Langmuir 1		$\frac{C_{eq}}{q_{eq}} = \frac{1}{q_m} C_{eq} + \frac{1}{K_L q_m}$	$\frac{C_{eq}}{q_{eq}}$ vs C_{eq}
Langmuir 2	$q_{eq} = \frac{q_m K_L C_{eq}}{1 + K_L C_{eq}}$	$\frac{1}{q_{eq}} = \left(\frac{1}{K_L q_m}\right)\frac{1}{C_{eq}} + \frac{1}{q_m}$	$\frac{1}{q_{eq}}$ vs $\frac{1}{C_{eq}}$
Langmuir 3		$q_{eq} = q_m - \left(\frac{1}{K_L}\right)\frac{q_{eq}}{C_{eq}}$	q_{eq} vs $\frac{q_{eq}}{C_{eq}}$
Langmuir 4		$\frac{q_{eq}}{C_{eq}} = K_L q_m - K_L q_{eq}$	$\frac{q_{eq}}{C_{eq}}$ vs q_{eq}
Redlich−Peterson	$q_{eq} = \frac{AC_{eq}}{1 + BC_e^g}$	$\ln\left(A\frac{C_{eq}}{q_{eq}} - 1\right) = g \ln(C_{eq}) + \ln(B)$	$\ln\left(A\frac{C_{eq}}{q_{eq}} - 1\right)$ vs $\ln(C_{eq})$

between the experimental and the predicted data points, it provides a numerical measure to interpret the goodness of fit of a given mathematical model to the data. Another well-known criteria which has a general purpose for goodness of fit of experimental data with isotherm models is the coefficient of determination (R^2):[36]

$$R^2 = \sum (q_{e,exp} - \bar{q}_{calc})^2 / \sum ((q_{e,exp} - \bar{q}_{calc})^2 + (q_{e,exp} - q_{calc})^2) \quad (4)$$

Kinetic Study. To understand the mechanism of the biosorption process, a kinetic study is helpful. One important kinetic aspect of any process is to determine the rate-determining step (RDS). Providing that the agitation rate is fast enough, solutes have no limit to reach the vicinity of the sorbent, and this cannot be the RDS. Thus, the RDS results from other phenomena including the following: (1) diffusion through the boundary layer to the surface of the adsorbent (external diffusion), (2) sorption of ions onto sites, and (3) intraparticle diffusion into the interior of the adsorbent.[16,29,37] It is usually observed that intraparticle diffusion is the RDS, and this normally can be tested using the equation described by the intraparticle model:

$$q_t = t^{0.5} \cdot K_p + C \quad (5)$$

where q ($mg \cdot g^{-1}$) is the amount adsorbed at time t, K_p is the intraparticle rate constant ($mg \cdot g^{-1} \cdot min^{-1/2}$), and C is a constant. To determine the order of kinetics, data were also fitted to two well-known kinetic models, that is, Lagergren pseudofirst-order and the pseudosecond-order.

The Lagergren pseudofirst-order (eq 6) and pseudosecond-order kinetic (eq 7) models can be written as:

$$q_t = q_e[1 + \exp(-k_1 t)] \quad (6)$$

$$q_t = \frac{k_2 q_e^2 t}{(1 + k_2 q_e t)} \quad (7)$$

where q_e and q_t are the sorbent capacity at equilibrium and time t, respectively. They are in terms of $mg \cdot g^{-1}$. The k_1 and k_2 are the rate constant of first- and second-order biosorption process (min^{-1} and $g \cdot mg^{-1} \cdot min^{-1}$), respectively.

Results and Discussion

Multivariate Optimization. Screening Design. Preliminary identification of significant factors was done by using a full 2^3 factorial design with three repeats at the center point. The results are listed in Table 3. It is clear that all of the main effects are significant ($P < 0.05$) and m has the greatest effect. It has a negative sign, which means increasing its level from low to high decreases the removal percentage. Table 4 illustrates the interaction between the main factors and reveals that there some interactions between m and s. The m, s, and pH are significant as well, but other interactions are insignificant at the selected significance level ($P < 0.05$) (Table 4). The presence of interaction means that the factors may affect the response interactively and not in an independent way; that is, their combined effect is greater or less than that expected for the straight addition of the effects.[19−21] For example, a negative interaction between m and s indicates that increasing the level of s has a less pronounced effect when m is at a low level than when at a high level. Figure 1 shows a normal probability of standardized effects. The basic theorem for use of the normal probability charts is that random effects can be expected to cluster along a line when plotted on normal probability paper. On the other hand, the effects of significant magnitude can be expected to fall off the "line of chance". Such a graph is constructed by plotting

Table 3. 2^3 Full Factorial Design Results

m	*s*	pH	*R* %
175	0.15	3.5	30
50	0.05	2	46
300	0.05	5	13
175	0.15	3.5	31
300	0.25	5	40
175	0.15	3.5	29
300	0.25	2	9
300	0.05	2	4
50	0.05	5	67
50	0.25	5	90
50	0.25	2	82

Table 4. Statistical Parameters for 2^3 Full Factorial Design

term	effect	coef.	SE coef.	*T*	*P*
constant		43.88	0.3536	124.1	<0.0001
m	−54.75	−27.38	0.3536	−77.43	<0.0001
s	22.75	11.38	0.3536	32.18	0.001
pH	17.25	8.63	0.3536	24.4	0.002
m·*s*	−6.75	−3.38	0.3536	−9.55	0.011
m·pH	2.75	1.37	0.3536	3.89	0.06[a]
s·pH	2.25	1.13	0.3536	3.18	0.086[a]
m·*s*·pH	8.75	4.37	0.3536	12.37	0.006
Ct Pt		−13.88	0.677	−20.5	0.002

[a] The parameters indicated are insignificant ($p > 0.05$).

the extent of the effects on the abscissa versus the cumulative probability function.[38,39] It is observed that all of the main factors and interactions just described as significant are far from the line of chance. This also confirms the results obtained in Table 4. There is also statistically significant curvature in the response surface ($P < 0.05$); therefore a simple flat plane is not representative of the experimental data, and one needs a multilevel design to obtain a more realistic model.

CCD Use for Optimization. A CCD with seven replicates at the center point and $\alpha = \pm 1.682$ was employed for optimization.[22,23] This design was rotatable. The rotatable design provides the desirable property of constant prediction variance at all points that are equidistant from the design center, thus improving the quality of the prediction.[19] The results are summarized in Table 5. The multiple regression

Table 5. CCD and Results Obtained

m	*s*	pH	*R* %
100.67	0.21	2.61	55.0
249.33	0.21	2.61	10.4
249.33	0.09	2.61	8.0
175.00	0.15	3.50	30.0
175.00	0.15	5.00	36.0
300.00	0.15	3.50	12.0
100.67	0.09	2.61	40.0
175.00	0.15	2.00	11.0
175.00	0.15	3.50	30.0
249.33	0.21	4.39	33.0
100.67	0.09	4.39	46.0
249.33	0.09	4.39	16.0
100.67	0.21	4.39	60.0
175.00	0.15	3.50	28.0
175.00	0.05	3.50	21.0
175.00	0.15	3.50	30.0
175.00	0.15	3.50	27.0
175.00	0.25	3.50	40.0
50.00	0.15	3.50	78.0
175.00	0.15	3.50	25.0

analysis of the resulting data led to the following model expressed as:

$$R = 67.5 - 0.599m + 14.6\text{pH} + 0.00109m^2 + 411s^2 - 2.00\text{pH}^2 - 0.986m{\cdot}s + 0.238m{\cdot}s{\cdot}\text{pH} \quad (8)$$

R represents the percent of Hg(II) removal efficiency.

The ANOVA results are illustrated in Table 6. It shows that the lack of fit is not significant ($P > 0.05$) and the regression is meaningful ($P < 0.05$). The estimated effects and coefficients are listed in Table 7. The residuals distribution is shown in Figure 2. According to the Ryan−Joiner (RJ) test, the residuals distribution is normal ($P > 0.05$).[38−40] The residuals distribution should also be checked for homoscedasticity and the presence of outliers.[18,19] If a point lies far from the majority, it may alert us about outlier(s). It was seen that the points are distributed in a random manner which verifies variance homogeneity. On the other hand, none of the points appear to be far from the others implying the

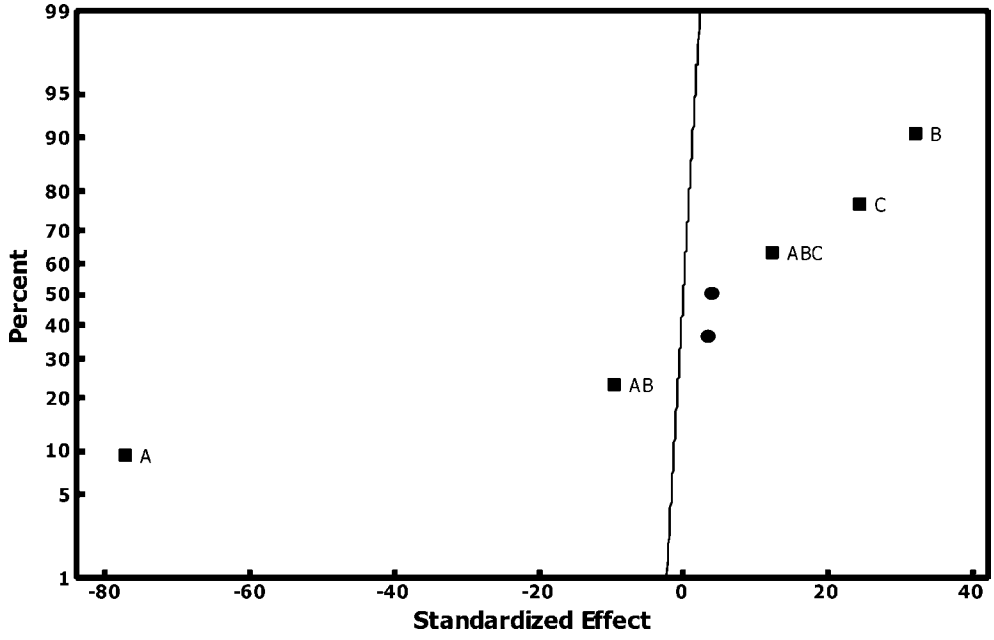

Figure 1. Normal probability plot for standardized effects with *R* as the response factor. ●, nonsignificant effects; ■, significant effects.

Table 6. Analysis of Variance (ANOVA) for the Suggested Model[a]

source	DF	SS	MS	*F*	*P*
regression	7	6046.48	863.78	121.33	< 0.0001
residual error	12	85.43	7.12		
lack of fit	7	64.1	9.16	2.15	0.209
pure error	5	21.33	4.27		
total	19	6131.91			

[a] DF = degree of freedom, SS = sum of square, MS = mean square, and *F* = F-test.

Table 7. Estimated Effects and Coefficients for the Suggested Third-Order Model

predictor	coef.	SE coef.	*T*	*P*
constant	67.45	13.28	5.08	< 0.00010
m	−0.5991	0.05181	−11.56	< 0.0001
pH	14.598	6.458	2.26	0.043
m^2	0.001088	0.000127	8.58	< 0.0001
s^2	410.9	109.3	3.76	0.003
pH^2	−1.9987	0.8805	−2.27	0.042
$m \cdot s$	−0.9863	0.2957	−3.34	0.006
$m \cdot s \cdot pH$	0.23848	0.06661	3.58	0.004

absence of outlier(s) (Figure 3). Figure 4a−c shows a three-dimensional (3-D) representation of *R* as a function of two independent variables, while the third is being kept at its founded optimum value. It is possible to find the optimum region through visual inspection of the surfaces. These surfaces also clearly show the interactions between the main factors: pH·*m*, pH·*s*, and *m*·*s*.

Model Validation and Optimum Conditions Assay. A model is valid when its predictions are reliable. The designed model has high adjusted R^2 (R^2(adj) = 97.8 %), and only about 2.2 % of total variances cannot be explained by the model. To examine whether the model has been overfitted or not, seven randomly designed runs that have not been used in model construction were evaluated with the model coefficients

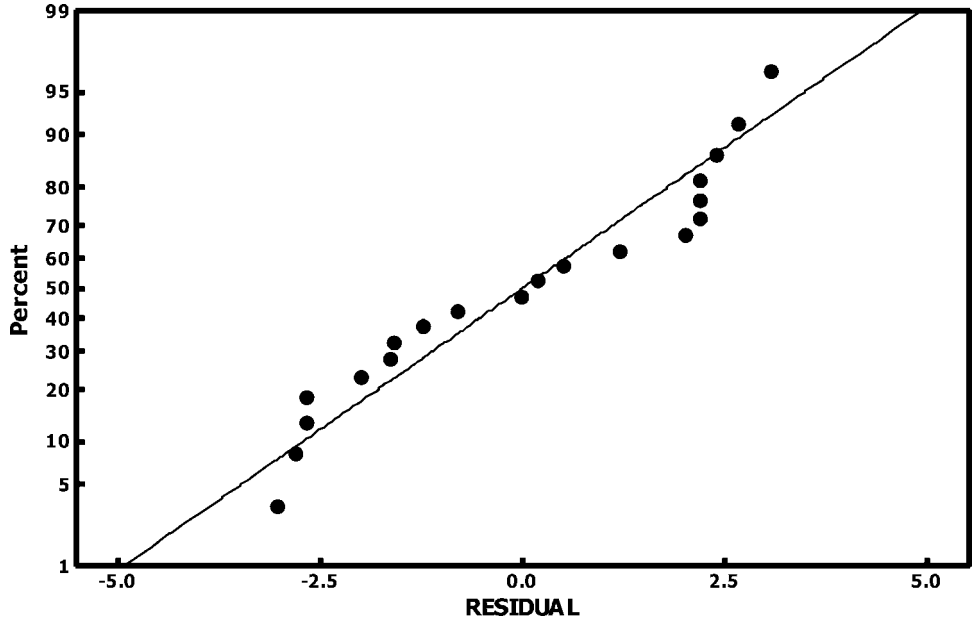

Figure 2. Normal probability plot for residuals. RJ = 0.963, *P*-value > 0.100.

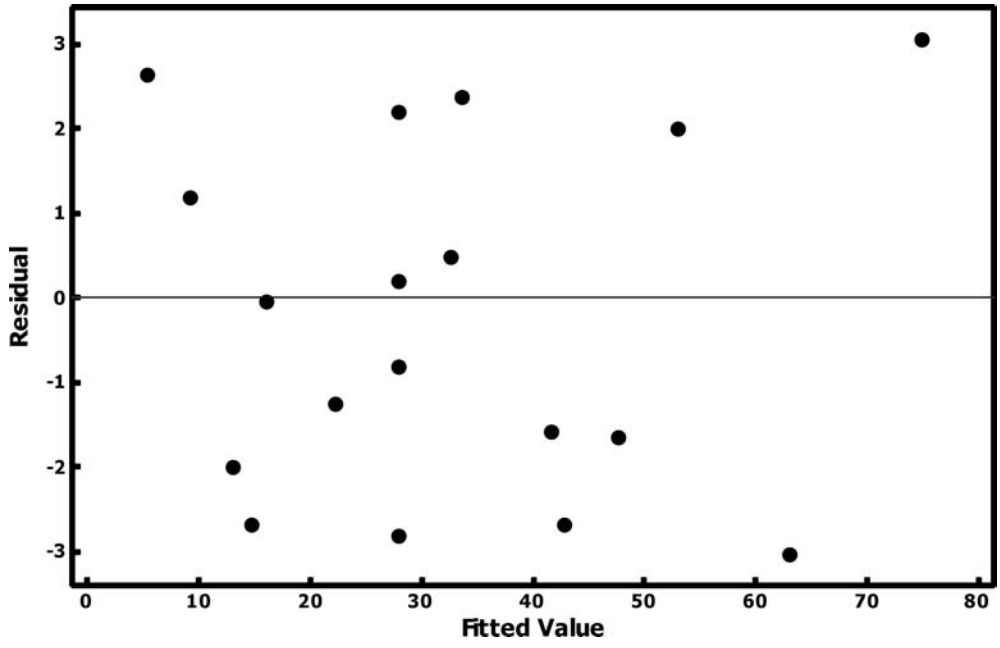

Figure 3. Standardized residuals vs plotted fitted values.

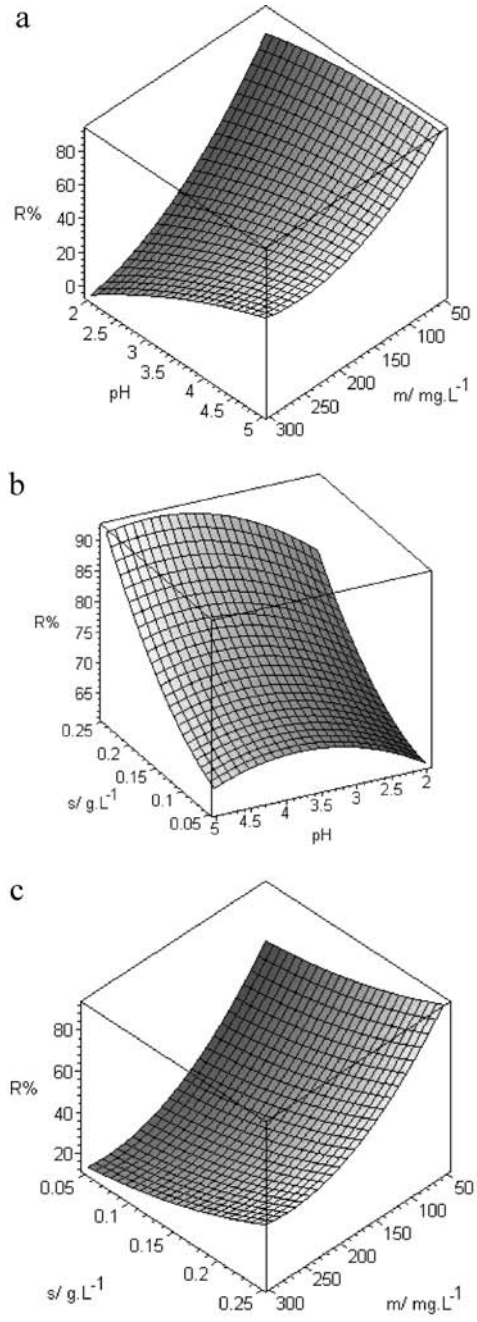

Figure 4. Response surface plots showing: (a) The effect of Hg(II) concentration (*m*) and pH and their mutual effect on *R* while the biomass amount was kept constant at its optimum value. (b) The effect on amount of sorbent (*s*) and pH and their mutual effect on the *R* while the Hg(II) concentration was kept constant at its optimum value. (c) The effect on Hg(II) concentration (*m*) and amount of sorbent (*s*) and their mutual effect on *R* while the pH was kept constant at its optimum value.

(Table 8). It was obvious that there is good agreement between theory and experiment.[29] This along with a high prediction R^2 (R^2(pred) = 94.84 %) confirms that the model has not been overfitted and has high predictability. Using the optimization toolbox of Maple, the best removal condition was calculated to be pH = 4.4, s = 0.25 g, and m = 50 mg·L^{-1} which corresponds to 92.25 % removal efficiency. The optimum conditions could also be derived from response surface 3-D plots. These surfaces, which visualize the predicted model equation, illustrate the optimum values of pH, *m*, and *s*. Three times replication of the experiment in optimum conditions gives an average of (90.0 ± 2.1) % which is in very good agreement with theory.

Table 8. List of Randomly Designed Experiments, Observed Responses, and Predicted Ones Using the Constructed Model

m	*s*	pH	predicted *R* %[a]	observed *R* %
160	0.2	4	41.3	40
75	0.1	3	56.6	57
125	0.1	3.5	38.5	40
220	0.25	5	48.4	47.5
50	0.1	3	68.8	67
90	0.1	5	51.4	52
130	0.25	3.5	55.4	56.5

[a] *R* % stands for removal percent.

Isotherm Studies. It is assumed that nonlinear regression has better performance than linear regression to obtain isotherm parameters.[34,36] This is because linearization may sometimes distort the error distribution structure of the isotherm.[35] In addition, avoiding linear transformation keeps the experimental data and isotherm parameters in the same *x* and *y* axis, making a comparison of isotherms more reliable.[34] Strictly speaking, original experimental data are plotted with q_{eq} as a function of C_{eq} for all of the isotherms considered, and the parameters are estimated in this space, while dependent and independent variables are altered depending on the linearization method used. To address the relevancy of this problem to the data presented here, a comparison was made between the results of linear and nonlinear regression.[34,36] Among the various linearized models used, the Langmuir (1) model has the lowest Δq and therefore better fitting. The complete fitness order is Langmuir (1) > Redlich-Peterson > Freundlich > Langmuir (2) > Langmuir (3) > Langmuir (4). A difficulty arises here because if the Langmuir (1) is selected, then it appears that it is the best fitted isotherm, while if Langmuir (3) or (4) is used, they will be the worst fitting isotherms (Table 9). On the other hand, if one uses R^2 as a measure to determine goodness of fit,[30] the order will be as: Langmuir (2) > Langmuir (1) > Redlich-Peterson > Langmuir (3) = Langmuir (4). When using the nonlinear regression, the Δq value was improved for all of the isotherms with respect to the corresponding ones in linear regression. So, the complete order of fitness is the Redlich−Peterson > Langmuir > Freundlich. A similar order is obtained if the R^2 of the nonlinear model is used as a statistical measure. According to the results obtained, one concludes that the above stated problem for linearization is relevant and therefore nonlinear regression is chosen as a superior parameter estimation method (Figures 5 and 6).[34,36]

Kinetic Study. The plotting of q_t versus $t^{0.5}$ showed multilinearity, implying that two or more steps have taken place.[16,29] The first, sharper portion is external surface adsorption or an instantaneous adsorption stage. The second portion is a gradual adsorption stage, where intraparticle diffusion is the rate-controlling step. The third portion is the final equilibrium stage where intraparticle diffusion starts to slow down due to low sorbate concentrations in the solution.[29,41] As shown in Figure 7, stage 1 is completed before 15 min, and the stage of intraparticle diffusion control (stage 2) begins and continues from (15 to 35) min. Finally, ultimate equilibrium adsorption (stage 3) starts after 35 min. Hg(II) is slowly transported via intraparticle diffusion into the particles and is finally retained in the micropores. In

Table 9. Comparison between Fitness of Linear and Nonlinear Regression Models

Regression Type: Linear						
isotherm	Langmuir 1	Langmuir 2	Langmuir 3	Langmuir 4	Freundlich	Redlich−Peterson
Δq	0.005886281	0.01308134	0.015516392	0.06436811	0.007689751	0.007055892
(R^2)	(0.9998)	(1.0)	(0.9939)	(0.9939)	(0.9328)	(0.9994)

Regression Type: Nonlinear			
isotherm	Langmuir	Freundlich	Redlich−Peterson
Δq	0.00576603	0.00653541	0.005411554
(R^2)	(0.946)	(0.932)	(0.954)

general, the slope of the line in stage 2 is called the intraparticle diffusion rate constant, k_p. The rate constant for intraparticle diffusion increased from (0.17 to 0.59) $mg \cdot g^{-1} \cdot min^{-1}$ with increasing Hg(II) concentration from (10 to 300) $mg \cdot L^{-1}$. The higher slope means a higher k_p and faster intraparticle diffusion. In addition, the results indicate that the intraparticle diffusion model fits the experimental data well for an initial period of the biosorption process. In addition the line did not pass through the origin. Therefore, it could be suggested that the mechanism of biosorption was complex and both external and intraparticle diffusion play a role in the actual biosorption process.[42] Applying nonlinear regression according to the Lagergren pseudofirst-order kinetic model did not give satisfactory fitness (data not shown, it has been also seen in our previous experience),[29] but a pseudosecond-order kinetic model yielded much better results with $\Delta q = 0$, for both (50 and 300) $mg \cdot L^{-1}$ Hg(II) initial concentration (Table 10). In accordance with the

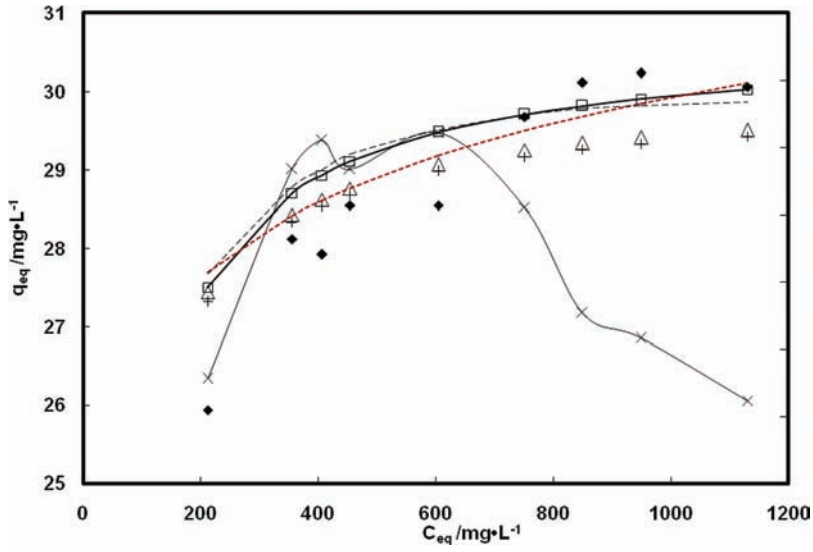

Figure 5. Isotherms obtained using the linear method for the adsorption of Hg(II) onto *Fraxinus* tree leaves. □, linear Langmuir 1; △, linear Langmuir 2; +, linear Langmuir 3; ×, linear langmuir 4; - - -, linear Freundlich; ——, linear Redlich−Peterson; ◆, experimental value.

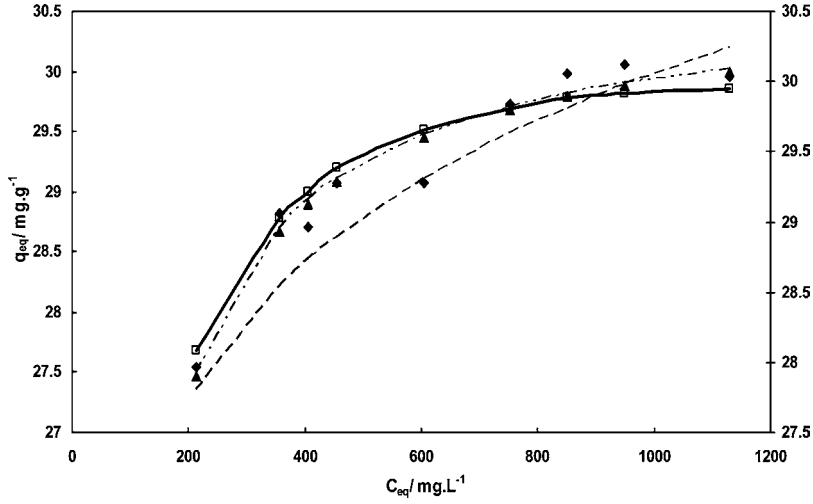

Figure 6. Comparison between isotherms obtained using linear and nonlinear regression methods. ◆, experimental value; —••—, linear Langmuir 1; □, linear Redlich-Peterson; —, nonlinear Redlich; - - -, nonlinear Freundlich; ▲, nonlinear Langmuir.

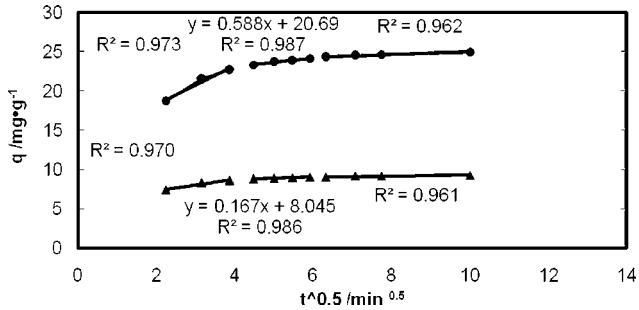

Figure 7. Intraparticle diffusion plot of Hg(II) sorption onto *Fraxinus* tree leaves. ▲, 50 mg·L^{-1}; ●, 300 mg·L^{-1}.

Table 10. Kinetic Parameters of Pseudosecond Order and Intraparticle Diffusion at Two Concentration Levels

	pseudosecond order				intraparticle diffusion		
initial concen.	K_2	q_{eq}					
mg·L^{-1}	min^{-1}	mg·g^{-1}	SD	R^2	k_p	c	R^2
10	0.08	9.37	0.0	1	0.17	8.04	0.987
300	0.022	25.38	0.0	1	0.59	20.67	0.987

pseudosecond-order reaction mechanism, the overall rate of Hg(II) sorption processes may be controlled by chemical processes, through the sharing of electrons between biosorbent and sorbate, or covalent forces, through the exchange of electrons between the particles involved.[42,43] It should be noted that the mechanism of the biosorption is a complex process and cannot be proven only by kinetic data and further studies are required. Table 11 shows the comparison of the q_m value for biosorption of Hg(II) on different biosorbents in the literature.[44−46] As can be seen the capacity for *Fraxinus* tree leaves, the uptake of Hg(II) is considerable and favorable due to its abundance, very low cost, and lack of need for generation.

Table 11. Comparison of Biosorption Capacity (q_{max}) *Fraxinus* Tree Leaves for Hg(II) with Other Biosorbents

sorbent	pH	q_{max} mg·g^{-1}	ref
treated sawdust (*Acacia arabica*)	6	20.6	44
Cyclotella cryptica	4	11.9	45
Scenedesmus subspicatus	4	9.2	45
camel bone charcoal	2	28.2	46
Fraxinus tree leaves	4.4	29.5	present study

Table 12. FT-IR Spectral Characteristics of *Fraxinus* Peaks Which Are Absent in Pristine Biomass or Change Their Position after Hg(II) Loading

	absorption band before adsorption	absorption band after adsorption	difference	
IR peak	cm^{-1}	cm^{-1}	cm^{-1}	assignment
1	1076	1053	23	C−O
2	absent	1159		C−O
3	1246	1240	6.0	CN stretching
4	1313	1323	10	C−O−C
5	absent	1373		CH_3 stretching
6	1417	1439	22	CH_2 bending
7	absent	1541		secondary amine group
8	1651	1653	2.0	C═O
9	3379	3385	6.0	OH, NH

FT-IR and XRD Study. FT-IR spectroscopy was used to obtain information on the nature of possible interaction between the functional groups of *Fraxinus* tree leaves and Hg(II). The FT-IR spectra of dried unloaded sorbent (A) and Hg(II)-loaded sorbent (B) are shown in Figure 8A,B. As can be seen, these spectra clearly show three peaks which indicate both changes in intensity and shift in wavenumbers. The relative shift and change in intensity of the stretching band at about (3379 to 3385) cm^{-1} is due to indicative −OH and −NH groups. The shift of the vibration band of carboxyl groups (−C═O) from (1651 to 1653) cm^{-1}, and stretching band of alcohols and carboxylic acids (C−O) from (1076 to

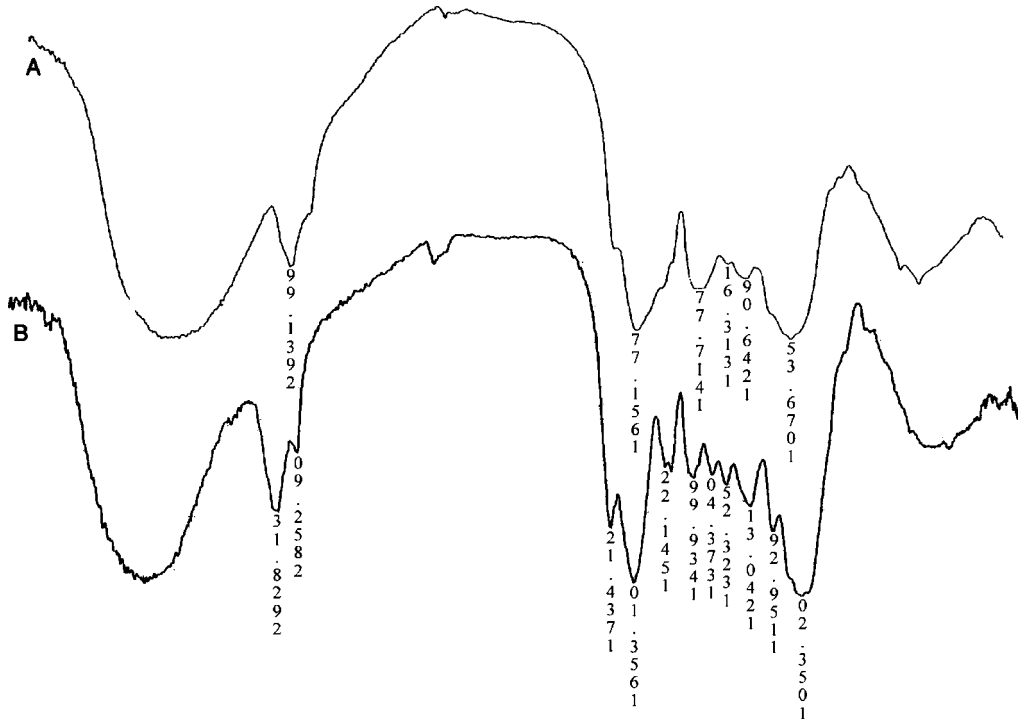

Figure 8. FT-IR spectra of pristine (A) and Hg(II) loaded biosorbent (B).

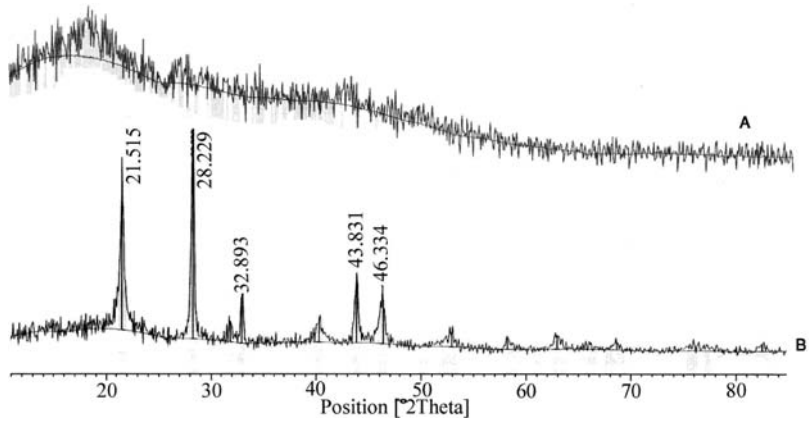

Figure 9. XRD spectra of pristine and Hg(II) loaded sorbent.

1053.20) cm^{-1} are also seen. The appearance of three new peaks after loading Hg(II) in (1159, 1373, and 1541) cm^{-1} clearly show that the functional groups C—O, CH_3-stretching, and secondary amines, respectively, are involved (Figure 8b). A remarkable change occurs in the fingerprint region of the spectrum. This part of the spectrum for unloaded (A) and loaded biosorbent (B) is different. Finally, the comparison of the FT-IR spectrum of unloaded sorbent (A) and loaded sorbent (B) show the changing and shifting of all indicated bands which confirm that most functional groups present of the sorbent are involved with Hg(II) during the biosorption process. All spectral information including the location of peaks and their possible assignment are given in Table 12. The change in position, appearance, or disappearance of some peaks is related to their involvement in the biosorption process.[16,47−50] A Philips powder X-ray diffractometer was used to study the solid-state morphology of pristine and Hg(II) loaded biosorbent. X-rays of a 1.5406 Å wavelength were generated by a Cu Kα source, and diffracted rays were detected by a Giger-Muller detector. The angle of diffraction was changed from (10 to 85)° to identify crystal structure of the biosorbent before and after biosorption (Figure 9). As can be seen, there is no peak in the spectrum of the native biosorbent, implying an amorphous nature. In contrast, there are several sharp peaks in the Hg(II) loaded sorbent with peaks at $2\theta = 21.515°$ and 28.229° as the most intense ones. This was attributed to the semicrystalline structure of the Hg(II) loaded biosorbent. The existence of a semicrystalline structure after adsorption may be an indication of the possibility of nucleation processes or complex formation between the functional groups present in the biosorbent with Hg(II) and also may be partially due to hydration.[47]

Conclusion

Hg(II) was successfully adsorbed by *Fraxinus* tree leaves, and the equilibrium data were better described by a nonlinear regression of the original isotherm rather than a linear regression applied to transformed and linearized isotherms. A kinetic study suggested a chemisorption mechanism for the biosorption rather than physical adsorption. An XRD pattern was also utilized, and it verified the mechanism suggested by the kinetic study. CCD as a response surface methodology was applied to find a suitable model for describing the removal efficiency. The optimum conditions were also found.

Acknowledgment

The authors would like to thank Dr. A. Zolanvari for his contribution and running the XRD spectrum.

Note Added after ASAP Publication: This paper was published ASAP on September 26, 2010. The Table 4 footnote was updated. The revised paper was reposted on October 7, 2010.

Literature Cited

(1) Manahan, S. E. *Fundamentals of Environmental Chemistry*, 2nd ed.; Lewis Publishers: New York, 2001.
(2) Radojevic, M.; Bashkin, V. N. *Practical Environmental Analysis*, 2nd ed.; RSC Publishing: Cambridge, U.K., 2006.
(3) Reddad, Z.; Gerente, C.; Andres, Y.; Le Cloirec, P. Adsorption of Several Metal Ions onto a Low-Cost Biosorbent: Kinetic and Equilibrium Studies. *Environ. Sci. Technol.* **2002**, *36*, 2067–2073.
(4) Volskey, B. *Sorption and Biosorption*; BV Sorbex, Inc.: Montreal, Canada, 2003.
(5) Al Rmalli, S. W.; Dahmani, A. A.; Abuein, M. M.; Gleza, A. A. Biosorption of mercury from aqueous solutions by powdered leaves of castor tree (*Ricinus communis L.*). *J. Hazard. Mater.* **2008**, *152*, 955–959.
(6) Schneide, I. A. H.; Rubio, J.; Misra, M.; Smith, R. W. *Eichhornia crassipes* as biosorbent for heavy metal ions. *Miner. Eng.* **1995**, *8*, 979–988.
(7) Sangi, M.; Shahmoradi, A.; Zolgharnein, J.; Azimi, G. H.; Ghorbandoost, M. Removal and recovery of heavy metals from aqueous solution using *Ulmus carpinifolia* and *Fraxinus excelsior* tree leaves. *J. Hazard. Mater.* **2008**, *155*, 513–522.
(8) Zolgharnein, J.; Shamoradi, A.; Sangi, M. R. Optimization of Pb(II) biosorption by *Robinia* tree leaves using statistical design of experiments. *Talanta* **2008**, *76*, 528–532.
(9) Dushenkov, V.; Nanda Kumar, P. B. A.; Motto, H.; Raskin, I. Rhirofiltration: the use of plants to remove heavy metals from aqueous systems. *Environ. Sci. Technol.* **1995**, *29*, 1239–1245.
(10) Wang, G. X.; Fuerstenau, M. C.; Smith, R. W. Removal of metal ions by nonliving water hyacinth roots. *Miner. Metall. Process.* **1999**, *16*, 41–47.
(11) Saeed, A.; Akhtar, M. W.; Iqbal, M. Removal and recovery of heavy metals from aqueous solution using papaya wood as a new biosorbent. *Sep. Purif. Technol.* **2005**, *45*, 25–31.
(12) Volesky, B. Removal and recovery of heavy metals by biosorption. In *Biosorption of Heavy Metals*; Volesky, B., Ed.; CRC Press, Inc.: Boca Raton, FL, 1990; pp 7−43.
(13) Macchi, G.; Marani, D.; Tirivanti, G. Uptake of mercury by exhausted coffee grounds. *Environ. Technol. Lett.* **1986**, *7*, 431–444.
(14) Chen, J. Z.; Tao, X. C.; Xu, J.; Zhang, T.; Lin, Z. L. Biosorption of lead, cadmium and mercury by immobilized *Microcystis aeruginosa* in column. *Process Biochem. (Oxford, U.K.)* **2005**, *40*, 3675–3679.
(15) Das, S. K.; Das, A. R.; Guha, A. K. A Study on the Adsorption Mechanism of Mercury on *Aspergillus versicolor* Biomass. *Environ. Sci. Technol.* **2007**, *41*, 8281–8287.

(16) Basha, S.; Murthy, Z. V. P.; Jhaa, B. Sorption of Hg(II) onto *Carica papaya*: Experimental studies and design of batch sorber. *Chem. Eng. J.* **2008**, *147*, 226–234.
(17) Lacher, C.; Smith, R. W. Sorption of Hg(II) by *Potamogeton natans* dead biomass. *Miner. Eng.* **2002**, *15*, 187–191.
(18) Zolgharnein, J.; Adhami, Zh.; Shahmoradi, A.; Mousavi, S. N. Optimization of removal of methylene blue by *Platanus* tree leaves using response surface methodology. *Anal. Sci.* **2010**, *26*, 111–116.
(19) Massart, D. L.; Vandeginste, B. G. M.; Buydens, L. M. C.; Jong, S. D. E.; Lewi, P. J.; Smeyers Verbeke, J. *Handbook of chemometrics and qualimetrics*, part A; Elsevier: Amsterdam, 2003.
(20) Bruns, R. E.; Scarmino, I. S.; de Barros Neto, B. *Statistical design-Chemometrics*, 1st ed.; Elsevier: Amsterdam, 2006.
(21) Montgomery, D. C. *Design and analysis of experiments*, 5th ed., Wiley: New York, 2001.
(22) Bezerra, M. A.; Santelli, R. E. E.; Oliveira, P.; Villar, L. S.; Esclaleira, L. A. Response surface methodology (RSM) as a tool for optimization in analytical chemistry-review. *Talanta* **2008**, *76*, 965–977.
(23) Ferreira, S. L. C.; dos Santoz, W. N. L.; Quintella, C. M.; Neto, B. B.; Bosque-Sandra, J. A. Doehlert matrix: a chemometrics tool for analytical chemistry-review. *Talanta* **2004**, *63*, 1061–1067.
(24) Riccardo, L. Experimental design in chemistry: A tutorial. *Anal. Chim. Acta* **2009**, *652*, 161–172.
(25) Can, M. Y.; Kaya, Y.; Algur, O. F. Response surface optimization of the removal of nickel from aqueous solution by cone biomass of *Pinus sylvestris*. *Bioresour. Technol.* **2006**, *97*, 1761–1765.
(26) Brasil, J. L.; Ev, R.; Milcharek, C. D.; Martins, L. C.; Pavan, F. A.; dos Santos, A. A., Jr.; Dias, S. L. P.; Dupont, J.; Zapata Norena, C. P.; Lima, E. C. Statistical design of experiments as a tool for optimizing the batch conditions to Cr(VI) biosorption on *Araucaria angustifolia* wastes. *J. Hazard. Mater* **2006**, *B133*, 143–153.
(27) Zulkali, M. M. D.; Ahmad, A. L.; Norulakmal, N. H. *Oryza sativa* L. husk as heavy metal adsorbent: Optimization with lead as model solution. *Bioresour. Technol.* **2006**, *97*, 21–25.
(28) Garg, U. K.; Kaur, M. P.; Garg, V. K.; Sud, D. Removal of nickel(II) from aqueous solution by adsorption on agricultural waste biomass using a response surface methodological approach. *Bioresour. Technol.* **2008**, *99*, 1325–1331.
(29) Zolgharnein, J.; Shahmoradi, A. Adsorption of Cr(VI) onto *Elaeagnus* tree leaves; Statistical Optimization, Equilibrium Modeling and Kinetic Studies. *J. Chem. Eng. Data* **2010**, *55*, 3428–3437.
(30) Zolgharnein, J.; Adhami, Zh.; Shahmoradi, A.; Mousavi, S. N.; Sangi, M. R. Multivariate optimization of Cd(II) biosorption onto *Ulmus* tree leaves from aqueous wastes. *Toxicol. Environ. Chem.* **2010**, *92* (8), 1461–1470.
(31) Sari, A.; Tuzen, M. Biosorption of total chromium from aqueous solution by red algae (*Ceramium virgatum*): Equilibrium, kinetic and thermodynamic studies. *J. Hazard. Mater.* **2008**, *160*, 349–355.
(32) Ho, Y. S.; Porter, J. F.; Mckay, G. Equilibrium isotherm studies for the sorption of divalent metal ions onto peat: copper, nickel and lead single component systems. *Water, Air, Soil Pollut.* **2002**, *141*, 1–33.
(33) Ho, Y.-S.; Chiu., W.-T.; Wang, C.-C. Regression analysis for the sorption isotherms of basic dyes on sugarcane dust. *Bioresour. Technol.* **2005**, *96*, 1285–1291.
(34) Kinniburgh, D. G. General purpose adsorption isotherms. *Environ. Sci. Technol.* **1986**, *20*, 895–904.
(35) Harrison, F.; Kati, S. K. Hazard of linearization of Langmuir's model. *Chemom. Intell. Lab. Syst.* **1990**, *9*, 249–255.
(36) Kumar., K. V.; Porkodi, K.; Rocha, F. Comparison of various error functions in predicting the optimum isotherm by linear and non-linear regression analysis for the sorption of basic red 9 by activated carbon. *J. Hazard. Mater.* **2008**, *150*, 158–165.
(37) Wu, F.-C.; Tseng, R.-L.; Juang, R.-S. Kinetic modeling of liquid-phase adsorption of reactive dyes and metal ions on chitosan. *Water Res.* **2001**, *35*, 613–618.
(38) Miller, J. N.; Miller, J. C. *Statistics and Chemometrics for Analytical Chemistry*, 4th ed.; Dorset Press: Dorchester, 2000.
(39) Filliben, J. J. The Probability Plot Correlation Coefficient Test for Normality. *Technometrics* **1975**, *17*, 111–117.
(40) Ryan, T. A.; Joiner, B. L., Jr. *Normal Probability Plots and Tests for Normality*, Technical Report; Statistics Department, The Pennsylvania State University: University Park, PA, 1976.
(41) Wang, B.-E.; Hu, Y.-Y.; Xie, L.; Peng, K. Biosorption behavior of azo dye by inactive CMC immobilized *Aspergillus fumigatus* beads. *Bioresour. Technol.* **2008**, *99*, 794–800.
(42) Ho, Y. S.; McKay, G. The kinetics of sorption of divalent metal ions onto sphagnum moss peat. *Water Res.* **2000**, *34*, 735–742.
(43) Lu, S.; Gibb, S. W. Copper removal from wastewater using spent-grain as biosorbent. *Bioresour. Technol.* **2008**, *99*, 1509–1517.
(44) Meena, A. K.; Kadirvelu, K.; Mishra, G. K.; Rajagopal, C.; Nagar, P. N. Adsorptive removal of heavy metals from aqueous solution by treated sawdust (*Acacia arabica*). *J. Hazard. Mater.* **2008**, *150*, 604–611.
(45) Schmitt, D.; Müller, A.; Csögör, Z.; Frimmel, F. H.; Posten, C. The adsorption kinetics of metal ions onto different tmicroalgae and siliceous earth. *Water Res.* **2001**, *35*, 779–785.
(46) Hassan, S. S. M.; Awwad, N. S.; Aboterik, A. H. A. Removal of mercury(II) from wastewater using camel bone charcoal. *J. Hazard. Mater.* **2008**, *154*, 992–997.
(47) Xu, H.; Liu, Y. Mechanisms of Cd^{2+}, Cu^{2+} and Ni^{2+} biosorption by aerobic granules. *Sep. Purif. Technol.* **2008**, *58*, 400–411.
(48) Sarı, A.; Tuzen, M. Biosorption of cadmium(II) from aqueous solution by red algae (*Ceramium virgatum*): Equilibrium, kinetic and thermodynamic studies. *J. Hazard. Mater.* **2008**, *157*, 448–454.
(49) Sari, A.; Tuzen, M. Removal of mercury(II) from aqueous solution using moss (*Drepanocladusrevolvens*) biomass: Equilibrium, thermodynamic and kinetic studies. *J. Hazard. Mater.* **2009**, *171*, 500–507.
(50) Tuzen, M.; Sari, A.; Mendil, D.; Soylak, M. Biosorptive removal of mercury(II) from aqueous solution using lichenb (*Xanthoparmelia conspersa*) biomass: Kinetic and equilibrium studies. *J. Hazard. Mater.* **2009**, *169*, 263–270.

Received for review June 5, 2010. Accepted September 10, 2010.

JE1006218